

# Narrowband-to-Broadband Conversions for SEVIRI

N. Clerbaux<sup>1</sup>, C. Bertrand, D. Caprion, B. Depaepe, S. Dewitte, L. Gonzalez, A. Ipe

*Royal Meteorological Institute of Belgium, Department of Observations, Section Remote Sensing from Space, Avenue Circulaire 3, B-1180 Brussels, Belgium.*

## Abstract

The possibility to estimate the broadband shortwave and longwave radiances from the narrowband measurements of the SEVIRI instrument is investigated. For this, a data base of corresponding SEVIRI and CERES broadband observations has been collected. The data base is then used to derive the narrowband-to-broadband regressions as well as to validate them. In general the regressions perform relatively well, with RMS error about 3.5% for shortwave and 0.7% for the longwave at regional scale (100x100km). However, important regression error is observed in some conditions like for example a desert dust over the ocean. So, the use of SEVIRI narrowband-to-broadband conversion for some specific situation should be done with caution and broadband observations (e.g. GERB) should be preferred if available.

## 1 Introduction

Estimation of the broadband shortwave and longwave radiances from the narrowband measurements of the SEVIRI instrument is needed for different applications such as: the improvement of the spatial resolution of TOA fluxes from the GERB instrument (Harries,2005), the derivation of GERB-like fluxes in the frame of the Climate Monitoring SAF (Caprion,2005), the estimation of energy flux incident on the ocean and land surface in the OSI (Le Borgne,2004) and LSA (Geiger, 2005) SAFs. For most of these usages, the GERB broadband observations can not be used directly because GERB does not have operational status on MSG-1 (but will be an operational mission on MSG-2,-3 and -4). Furthermore, at time of reading, we are still working on the official release of GERB data.

The possibility to derive TOA radiative fluxes from SEVIRI has been theoretically studied in (Clerbaux,2001) which reports narrowband-to-broadband conversion RMS errors of 3.2% and 0.7% for shortwave and longwave radiation, respectively. This early work was based on NB and BB radiances simulated by radiative transfer computation.

Since february 2004, a first SEVIRI instrument is operational and, in parallel, broadband observations are available about 4 times per day from the CERES instruments (Wielicki,1996) on board the Terra and Aqua polar orbiting satellites. In this study, those NB and BB observations are combined to derive empirical relations and to analyse their performance.

---

<sup>1</sup>Email: Nicolas.Clerbaux@oma.be

## 2 The Database of NB and BB observations

We used CERES ERBE-like (ES8) Edition-2 data for the FM2 (on Terra) and FM3 (on Aqua) instruments for the months of March, April and July 2004. In a first step, the CERES data which are coangular with the MSG direction of observation are selected. At this stage, "co-angular" means that the angle between the CERES and MSG direction of observations is less than  $15^\circ$ . In a second step, the SEVIRI data corresponding to the CERES observations are extracted provided the time difference between the 2 observations is less than 450 secondees. The CERES PSF is modelised using a circular point spread function (PSF) with radius of 6 SEVIRI pixels (about 18km at sub-satellite point). With those criteria, about 22 000 coangular BB and NB observations are extracted for each day and for each CERES instrument. For the 3 months and the 2 CERES instruments, the total number of couples of BB and NB observation reaches 4082203. The spatial homogeneousness  $\sigma$  in the neighbourhood of the observation is estimated by analysing the variation of the PSF averaged SEVIRI VIS  $0.6 \mu\text{m}$  value when the PSF is moved by  $+/- 3$  pixels in the vertical and horizontal directions. Let's denote  $L_{0.6,max}$  and  $L_{0.6,min}$  the maximal and minimal radiance reached in this neighbourhood, the spatial homogeneousness is evaluated as:

$$\sigma = \frac{(L_{0.6,max} - L_{0.6,min})}{(L_{0.6,max} + L_{0.6,min})/2} \quad (1)$$

For the longwave radiation, the  $\sigma$  is estimated from the IR  $10.8 \mu\text{m}$  radiance instead of the VIS  $0.6$ . For each pair of observation in the data base we also have a crude cloud cover identification via the ERBE classification associated to the CERES observation. The different ERBE cloud covers are: clear, partly cloudy, mostly cloudy and overcast.

## 3 Shortwave Radiation

### 3.1 Regressions

An extensive study of the best suited regressions has been performed using a least mean square software. It was decided to derive dedicated regressions for 5 types of surface: ocean, dark and bright vegetation, dark and bright desert. The classification of the Meteosat field-of-view according to these types is illustrated on figure (1). We have searched the more interesting predictors in the set  $\rho_{0.6}, \rho_{0.8}, \rho_{1.6}, \theta_0, \theta, \phi, \alpha, \beta$  to estimate the BB reflectance  $\rho_{bb}$ . For this study, and the derivation of the regression, a preliminary selection of the observations with relatively high spatial homogeneousness is performed: an ERBE clear observation is selected if  $\sigma < \sigma_{th,clear}$  while a ERBE cloudy observation is selected if  $\sigma < \sigma_{th,cloudy}$ . These thresholds are given in table (1) and are dependent on the surface type in order to have about half clear and half cloudy observations for each surface types. The coangular data are kept if the angle is less than  $3^\circ$ . Also, the risk of sun glint contamination is removed from the data base ( $\alpha < 25^\circ$ ).

Our findings were that: (i) the first predictor is the  $\rho_{0.6}$  reflectance, (ii) the  $\rho_{0.8}$  reflectance should be used to obtain good result over the clear vegetation, (iii) the  $\rho_{1.6}$  is not very helpful except for sandy surface, (iv) there is a small dependency in solar zenith angle  $\theta_0$ , (v) there is no significant dependency in  $\theta$  and  $\phi$ , at least when clear and cloudy data are processed together, (vi) there is a small dependency in the sun-glint angle  $\alpha$ , (vii) a second order term (like  $\rho_{0.6}^2$  is needed to avoid biais when only clear or cloudy conditions are considered . Given that, we decided to use the following formula for the shortwave narrowband-to-broadband conversion:

surface	total	max angle	$\sigma_{th,clear}$	$\sigma_{th,cloudy}$	clear	cloudy
ocean	2611413	3°	0.25	0.2	17395	19728
dark vege	442235	3°	0.25	0.2	3873	6876
bright vege	580511	3°	0.25	0.3	9780	14619
dark desert	117959	3°	0.2	0.5	3281	2221
bright desert	318493	3°	0.07	0.5	8441	5405

Table 1: For each surface type: original number of coangular observations in the database, selection criteria on the angle and spatial homogeneousness for clear and cloudy conditions, selected number of coangular observations for clear and cloudy conditions.

surface	$c_0$	$c_1$	$c_2$	$c_3$	$c_4$	$c_5$	$c_6$	RMS
ocean	0.015985	0.247134	0.004561	0.518540	0.015142	0.000129	0.000265	5.25%
dark vege.	0.007039	0.447929	-0.018466	0.373205	-0.007576	0.000379	0.000099	4.13%
bright vege.	0.006219	0.465640	-0.036540	0.359887	-0.011129	0.000357	0.000169	4.64%
dark desert	0.012397	0.403222	0.009855	0.398442	-0.028190	0.000207	0.000132	4.62%
bright desert	0.036945	0.238924	0.075104	0.477670	-0.069874	0.000566	0.000097	2.69%

Table 2: Regression parameters  $\{c_i\}$  f for the shortwave estimation with Eq. (2) and residual RMS error.

$$\rho'_{bb} = c_0 + c_1 \rho_{0.6} + c_2 \rho_{0.6}^2 + c_3 \rho_{0.8} + c_4 \rho_{1.6} + c_5 \theta_0 + c_6 \alpha \quad (2)$$

The Table (2) gives, for the 5 surface types the best fit parameters  $c_i$  and the residual RMS error [%].

### 3.2 Validations

As a first validation, we have applied the regression (2) to the entire data base of coangular observations (i.e. whatever is the spatial homogeneousness and with angle of observation up to 15°) and evaluated the bias:

$$bias = \frac{\langle \rho'_{bb} \rangle - \langle \rho_{bb} \rangle}{\langle \rho_{bb} \rangle} \quad (3)$$

which compares the average estimated  $\langle \rho'_{bb} \rangle$  and the average observed  $\langle \rho_{bb} \rangle$  broadband reflectances. The table (3) gives the bias for the 5 surface types and for all sky, clear sky (ERBE "clear" or "partly cloudy") and cloudy sky (ERBE "mostly cloudy" or "overcast") conditions. In average, the regressions perform very well with, in general, a small overestimation of the BB in clear conditions and underestimation in cloudy condition. The worse case being the cloudy ocean where the bias reaches -1.12% (underestimation.)

As a second validation we have analyzed the bias at regional scale (100 km). For this, the Meteosat field of view is segmented in boxes of 30 by 30 SEVIRI pixels over which the bias (Eq.3) is estimated. The left panels on Fig.(2) show the averaged measured BB reflectance  $\langle \rho_{bb} \rangle$  while the right panels give the images of the bias. Top, middle and bottom panels are for all-sky, clear-sky and cloudy-dky conditions,

surface type	all sky			clear sky			cloudy sky		
	num	$\langle \rho_{bb} \rangle$	bias	num	$\langle \rho_{bb} \rangle$	bias	num	$\langle \rho_{bb} \rangle$	bias
ocean	2133898	0.210	-0.68%	1363975	0.113	0.17%	769923	0.382	-1.12%
dark vege	407193	0.260	0.24%	223130	0.181	1.12%	184063	0.356	-0.30%
bright vege	551147	0.267	0.10%	365199	0.202	0.74%	185948	0.394	-0.54%
dark desert	115706	0.236	0.52%	99004	0.215	0.87%	16702	0.366	-0.68%
bright desert	311910	0.315	0.14%	273868	0.304	0.29%	38042	0.394	-0.70%

Table 3: Shortwave regression validation: bias (Eq. 3) for each surface type and for all sky, clear sky and cloudy sky conditions.

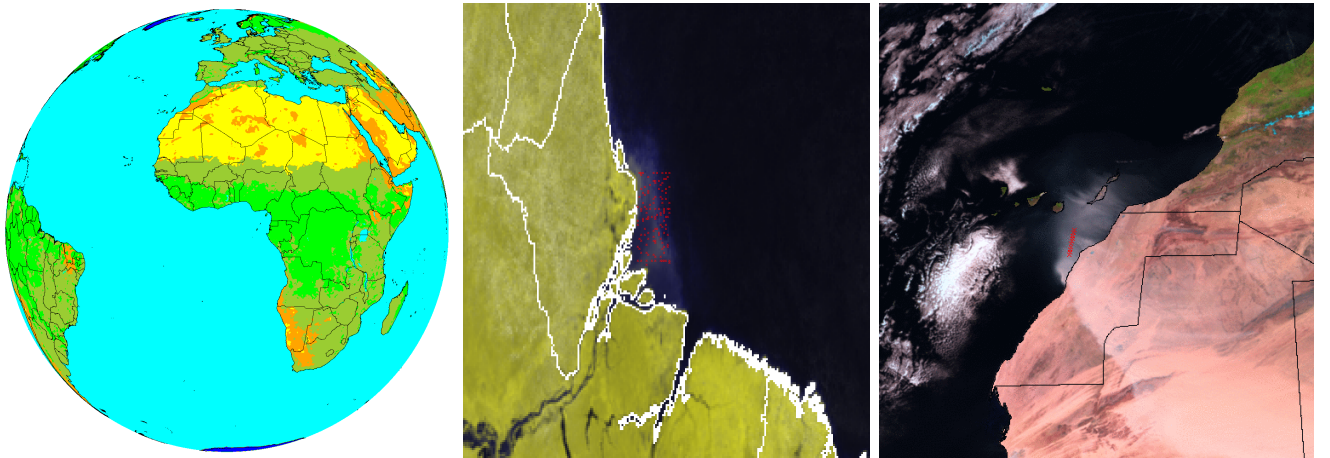


Figure 1: Surface type in the meteosat field of view (left) and localisation of the coangular data (red crosses) at the mouths of the Amazon river (center) and during the 3 March 2004 desert dust event (right).

respectively. In all-sky conditions there is nearly no bias. The clearsky condition is interesting to check if there remain surface type dependencies. The land surface is relatively well modelised with bias ranging between -3.5% and +3.5%. However, higher NB-to-BB error are observed over the ocean surface, typically about 5%, according to the angular geometry (higher at grazing observation angle and at the subsatellite point). The regression for the ocean appears also in error where non-standard ocean color exist such as at the mouths of the Amazon river (see Fig. 1, center) where the BB reflectance is overestimated of 13%. The same kind of problem is observed in case of desert dust cloud over the ocean (Fig. 1, right) where a bias of +13% is observed.

In summary, the shortwave regression performs well in most of the Meteosat field of view. However, higher narrowband-to-broadband conversio error are observed in case of: sun glint, aerosols, non-standard ocean color.

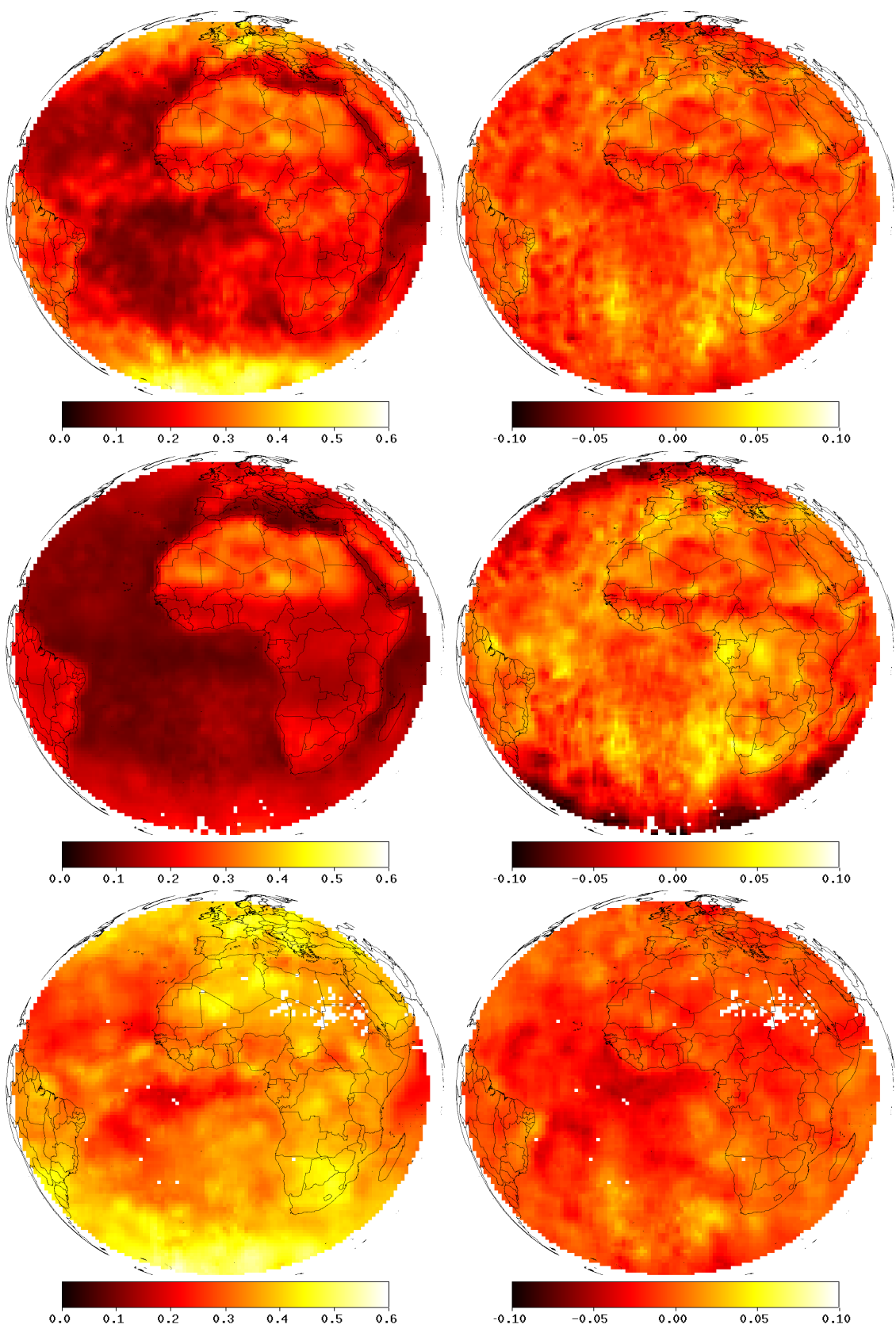


Figure 2: Shortwave regional bias: averaged BB radiance  $\langle \rho_{bb} \rangle$  (left) and bias (right) for all-sky (top), clear-sky (middle) and cloudy-sky (bottom) conditions.

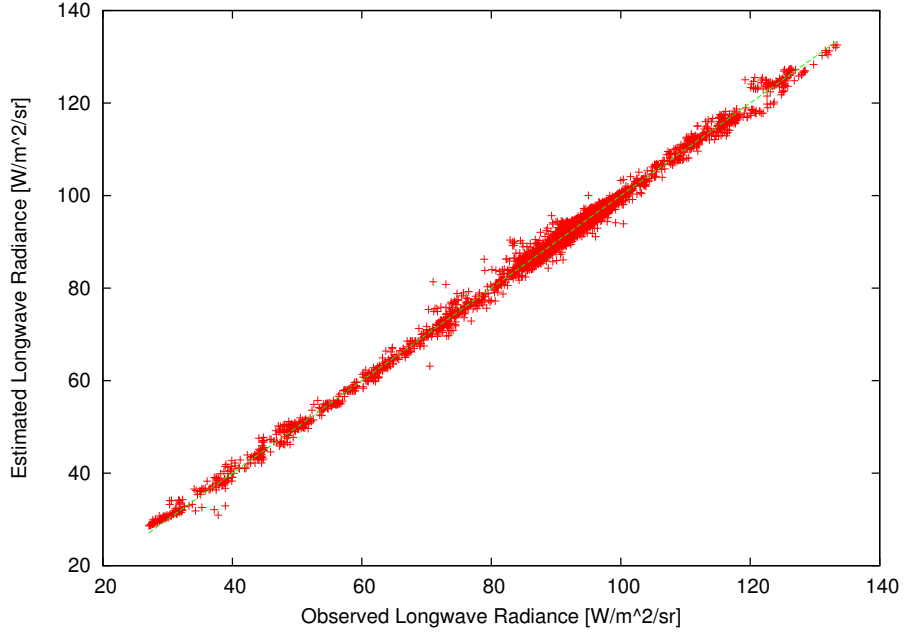


Figure 3: Scatter plot of the estimated LW radiance (with Eq. 4) according to the CERES measured radiance.

## 4 Longwave Radiation

### 4.1 Regressions

An extensive study of the best suited regression has been performed using a least mean square software. We have searched the more interesting predictor in the set  $L_{6.2}$ ,  $L_{7.3}$ ,  $L_{8.7}$ ,  $L_{9.7}$ ,  $L_{10.8}$ ,  $L_{12.0}$ ,  $L_{13.4}$ ,  $\theta$ , to estimate the BB radiance  $L_{bb}$ . To allow this study, a preliminary selection of the observations with relatively high spatial homogeneousness is done by selecting, for each  $5Wm^{-2}sr^{-1}$  bin of BB radiance, the 1000 observations having the less spatial dispersion. As for the shortwave, the coangular data are kept if the angle is less than  $3^\circ$ . From this study, we decided to simply select the following linear regression to estimate the broadband radiance from the narrowband radiances and the viewing zenith angle  $\theta$ :

$$L'_{bb} = 17.71 + 1.86L_{6.2} + 8.52L_{7.3} + 5.01L_{8.7} - 3.86L_{9.7} + 1.73L_{10.8} - 0.551L_{12} + 6.14L_{13.4} + 0.0166\theta \quad (4)$$

The figure (3) shows the scatter plot of the estimated BB versus the observed BB radiances. The residual error on the estimated BB is  $1.0Wm^{-2}sr^{-1}$  (or 1.1%). This value is a bit higher than the 0.7% reported in [Clerbaux,2001] but a part of the difference must be attributed to the empirical approach adopted here (colocalisation, coangularity,...).

## 4.2 Validations

As for the shortwave, the bias introduced by the NB-2-BB conversion is analyzed at regional scale. Results are given on Figure (4) for the all-sky, the clear-sky, the cloudy-sky. The day time and the night time conditions have also been analyzed but are not shown here. The figure show that the bias lies in the range [-0.5%:+0.5%], except for cold clouds where higher relative error can be observed.

## 5 Conclusions

Empirical regressions to estimate the BB shortwave and longwave radiances from the SEVIRI NB measurement of SEVIRI have been derived and validated. The associated RMS error can be estimated at 3.5% for the shortwave and 0.7% for the longwave, in good agreement with previous theoretical studies (Clerbaux, 2001). The RMIB GERB data processing will use these BB estimate to derive, in addition of the nominal GERB 50-km products, a set of products at the enhanced spatial resolution of 10 km. An interesting result of the study is that, although the regressions perform well in average, important error can be introduced over particular scene type such as a desert dust cloud.

## References

- [1] Clerbaux, N. and Dewitte, S. and Gonzalez, L. and Ipe, A. and Nicula, B. , (2001) Derivation of the Top Of The Atmosphere Radiative Fluxes from SEVIRI: Methodology, Accuracy and Perspectives., *Proc. of the 2001 EUMETSAT Meteorological Satellite Data User's Conference, Antalya*, pp 69–76.
- [2] Caprion, D. and Clerbaux, N. and Dewitte, S. and Bertrand, C. and Depaepe B. and Ipe, A. and Gonzalez, L, (2005) Initial Operation of the CM-SAF TOA Flux Products, *Proceedings of the 2005 Meteorological Satellite Conference, Dubrovnik*.
- [3] Geiger, B. and Lajas, D. and Franchisteguy, L. and Roujean, J-L. and Lanjeri, S. and Meurey, C. (2005) The Land-SAF Surface Albedo and Downwelling Shortwave Radiation Flux Products, *Proceedings of the 2005 Meteorological Satellite Conference, Dubrovnik*.
- [4] Harries, J.E. , (2005) The Geostationary Earth Radiation Budget Project, *Bulletin of the American Meteorological Society*, July 2005
- [5] Le Borgne, P. and Legendre, G. and Marsouin, A. (2004) METEOSAT And GOES-East Imager Visible Channel Calibration, *J. Atmos. Oceanic Technol.*, 21, 1701-1709.
- [6] Wielicki, B. A. and Barkstrom, B. R. and Harrison, E. F. and Lee III, R. B. and Smith, G. L. and Cooper, J. E. , (1996) Clouds and the Earth's Radiant Energy System (CERES): An Earth Observing System Experiment, *Bulletin of the American Meteorological Society*, 77, 853–868.

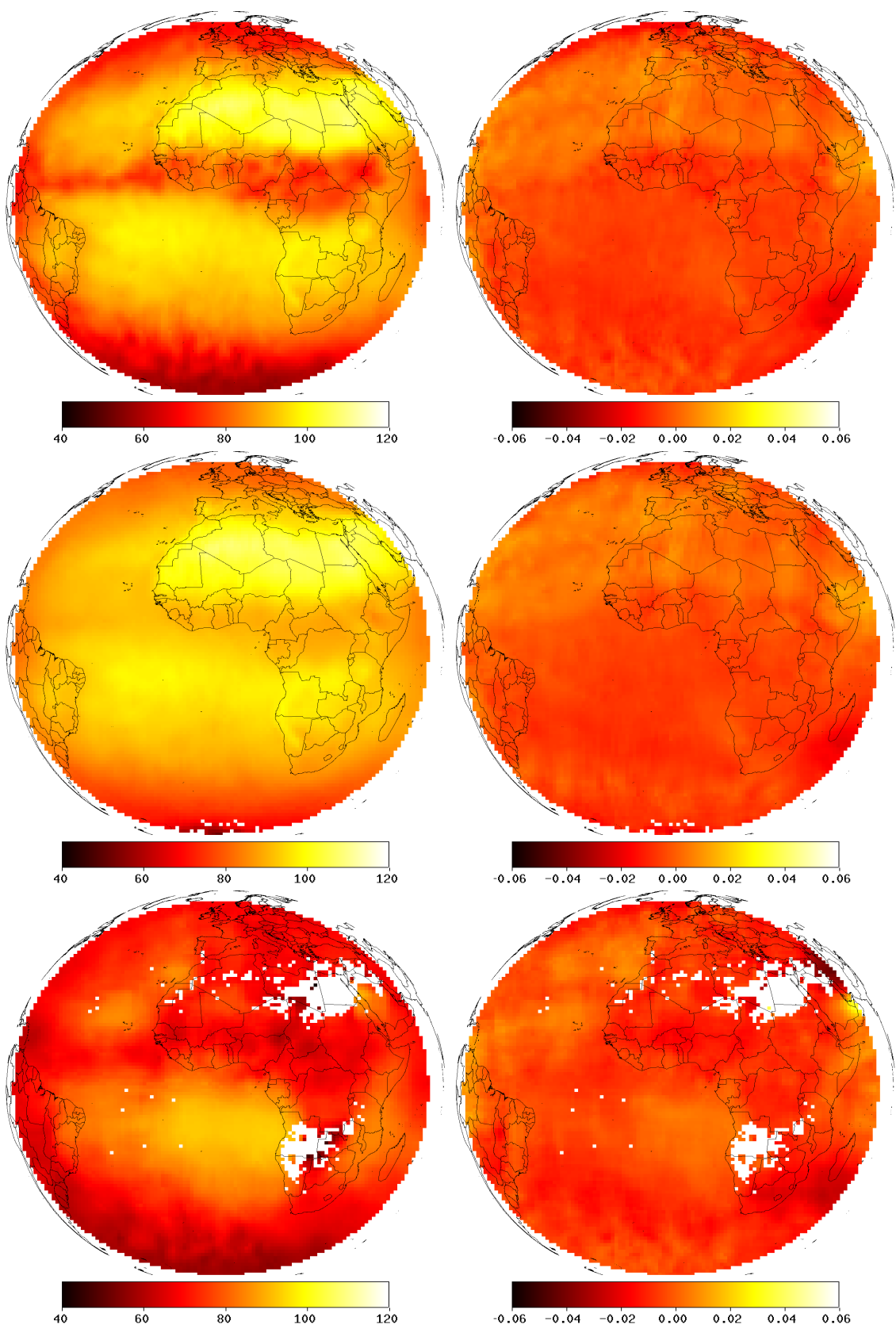


Figure 4: Longwave regional bias: averaged BB radiance  $\langle L_{bb} \rangle$  (left) and bias (right) for all-sky (top), clear-sky (middle) and cloudy-sky (bottom) conditions.